Imaging Recoil Ions from Optical Collisions between Ultracold, Metastable Neon Isotopes

B. Ohayon,[1,*] H. Rahangdale,[1] J. Chocron,[1] Y. Mishnayot,[1,2] R. Kosloff,[3] O. Heber,[4] and G. Ron[1]
[1]Racah Institute of Physics, Hebrew University, Jerusalem 91904, Israel
[2]Soreq Nuclear Research Center, Yavne 81800, Israel
[3]The Institute of Chemistry, The Hebrew University of Jerusalem, Jerusalem 91904, Israel
[4]The Weizmann Institute of Science, Rehovot 76100, Israel

(Received 20 April 2019; revised manuscript received 12 July 2019; published 6 August 2019)

We present an experimental scheme that combines the well-established method of velocity-map imaging with a cold trapped metastable neon target. The device is used for obtaining the branching ratios and recoil-ion energy distributions for the penning ionization process in optical collisions of ultracold metastable neon. The potential depth of the highly excited dimer potential is extracted and compared with theoretical calculations. The simplicity to construct, characterize, and apply such a device makes it a unique tool for the low-energy nuclear physics community, enabling opportunities for precision measurements in nuclear decays of cold, trapped, short-lived radioactive isotopes.

DOI: 10.1103/PhysRevLett.123.063401

Excited states of noble gases harbor sufficient energy to ionize most atoms and molecules upon collision. These reactive collisional processes play a crucial role in early Universe chemistry [1], and have been identified as important for the evolution of planetary atmospheres [2], and the chemistry of cold interstellar medium [3].

Noble gas atoms possess a long-lived *metastable* state that is amenable to the methods of laser cooling and trapping [4,5], leading to ultracold (<mK), dense ($>10^{10}/\mathrm{cm}^3$) samples, in which collisional processes occur predominantly in the quantum regime, where only a few partial waves contribute. However, a major difficulty arises for quantum mechanical calculations of these reaction processes, owing to the coupling of the entrance molecular channel to the ionization continuum [6], and the highly excited nature of the reactants [7].

An appreciable microscopic understanding of these reactions stems from an agreement between state of the art, relativistic *ab initio* potentials and ionization widths, and ample, precise experimental input. Experiments investigating single or dual species ultracold collisions usually measure trap loss and ionization rates [7–12], and in some implementations employ mass-spectroscopic techniques for separating the reaction products [13–16]. Thus, theoretical calculations, which have many degrees of freedom, are calibrated by comparing to a single, global quantity such as a reaction cross section or the branching ratio to an ionic species [17,18]. However, accurate determinations of the energy distributions of electrons and ions, routinely employed for molecular beams [19], offer a high-resolution window as to the involved potential energy surfaces (Fig. 1).

Modern determinations of charged fragments angle-resolved energy distributions usually rely on two

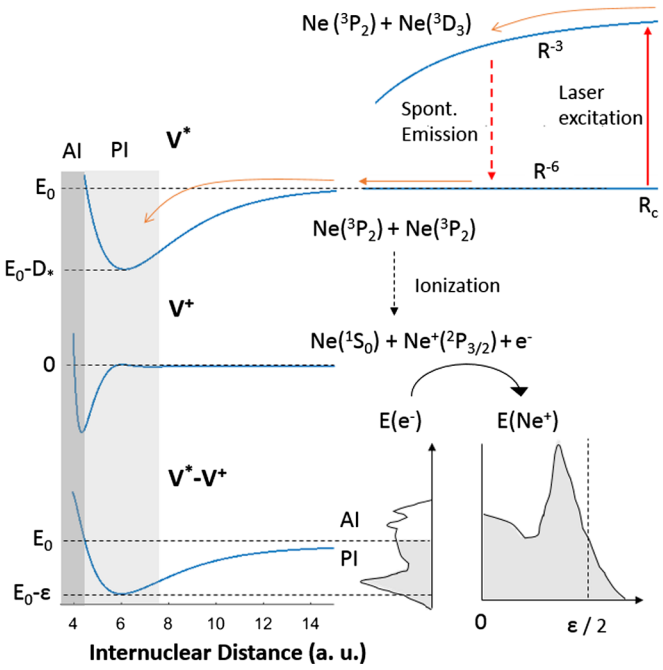

FIG. 1. Schematic representation of optically assisted collisions. Ultracold, metastable neon atoms are excited by near-resonant laser radiation from a weak van der Waals attraction, to a strong dipole-dipole attraction at a large internuclear distance R_c, where they accelerate until emitting a photon spontaneously. Associative ionization (AI) occurs in the dark shaded area of the difference potential and leads to electrons with energy higher than the available energy $E_0 = 12$ eV. Penning ionization (PI) occurs in the light shaded area and leads to electrons with energy lower than E_0. The lowest energy electrons, which correspond to the highest energy penning ions, result from ionization near the minimum of the difference potential and grant access to the potential depth $D_* \approx \epsilon$.

 © 2019 American Physical Society

powerful techniques: cold target recoil ion micrsocopy (COLTRIMS), reviewed in [20], and velocity map imaging (VMI) [21,22]. The merging of these methods with laser-cooling and trapping techniques offers substantial advantages over beam experiments and opens up new areas of research. Moreover, ultracold samples harbor the possibility of quantum-state preparation, and coherent control of collisional properties [23]. From a nuclear physics point of view, a cold, trapped, short-lived (typically $\tau = 0.1$–100 s) sample constitutes the ideal target for precision Beta- [24], and Beta-delayed-neutron [25] decay studies.

Owing to the aforementioned advantages, COLTRIMS has been successfully incorporated with a magneto-optical-trap (MOT) target to create the so-called MOTRIMS devices [26]. Nevertheless, the cost, complexity, and the level of involvement of its operation [27], as well as the inherently low rates and efficiencies [28], have limited the use of MOTRIMS to a few groups within the atomic and molecular physics community [29,30], and precluded it from being adopted by nuclear physicists.

In this Letter we report a successful implementation of a simple, efficient, MOT-VMI device. Utilizing its abilities, we report precise values for penning and associative ionization (PI and AI, respectively) branching ratios (BRs), as well as recoil-ion energy distribution from cold, optical collisions between trapped metastable neon isotopes. From the energy distributions we extract the potential well depth of the highly excited molecular potential, and compare with *ab initio* calculations and similar systems.

A traditional VMI setup consists of a repeller electrode, a gridless ring electrode acting as an electrostatic lens, and a gridless, grounded ring extractor [21]. The voltage difference between the repeller and extractor, along with the size and distance of the imaging detector, sets the scale of energies to be detected. The lens voltage and shape are optimized so as to cancel the effect of the finite source size. Particles with the same momentum, emerging from different locations within the target volume are imaged to the same location on the detector. Once the dynamic range is selected, the device is optimized by fine adjustment of the lens voltage. The energy resolution in most VMI setups is determined by the effective target volume, the quality of focusing, and the intrinsic resolution of the detection system. For low to medium (10 eV) energy charged particles, most reported values are in the range of $\Delta E/E = 1\%$–5%, which is accomplished here as well.

Figure 2 presents our adaptation of the VMI geometry to the magneto-optical-trap environment. The cooling and trapping setup includes a dynamically reconfigurable Zeeman-Slower [31], and a state- and isotope-selective deflection stage in [32]. For merging the VMI and the MOT, we elected to use the simple, cylindrically symmetric, three-electrode arrangement, where we merged the repeller with a flight tube for coincidence TOF detection.

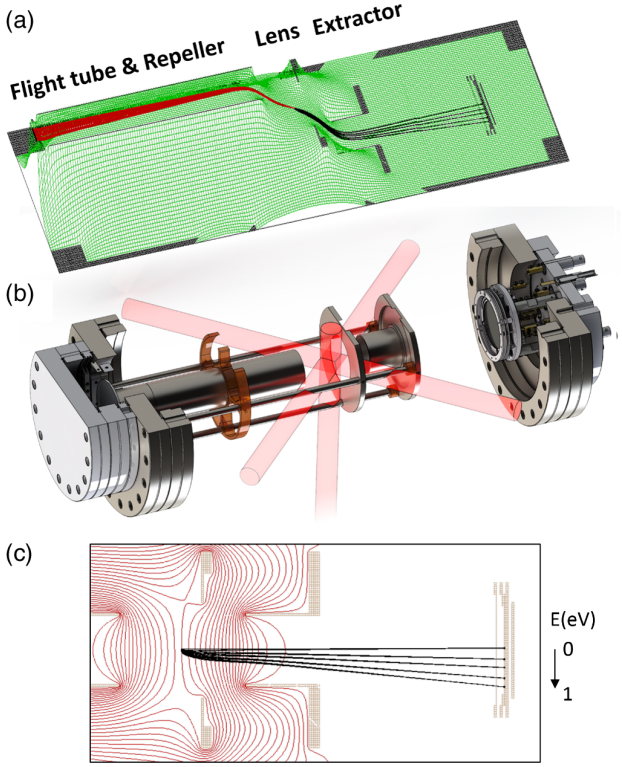

FIG. 2. The magneto-optical-trap VMI (MOT-VMI) setup. (a) SIMION 8.1 simulation of the trajectories of charged particles emerging from the trap volume in time-of-flight (TOF) mode of operation. At 4 kV deflection voltage, all ions (red trajectories) up to 1 eV reach the detector at the end of the flight tube, and all electrons up to 13 eV (black trajectories) reach the position sensitive detector. Electrical potential at the center plane is portrayed as a gravitational surface. (b) Computer assisted draft drawing of the implemented device. The trapping region is located in the intersection of the laser-cooling beams. (c) SIMION 8.1 simulation of ion trajectories in ion-imaging mode of operation. The ions emerge perpendicularly to the detector, from a 1 mm FWHM trap volume, grouped by initial energy of 0–1 eV, and focused to less than 200 μm on a position sensitive detector. Potential contours of 5 V spacing are indicated.

The radii and positions of various elements are optimized within the geometrical constraints of the MOT using the simulation package SIMION 8.1, to maximize the focusing capabilities for a variety of modes of operation.

The internal energy of cold, trapped metastable neon, $E^* = 17$ eV, exceeds the ionization potential E^+ of most atoms and molecules. The ionization reaction between a metastable noble atom Rg* and a molecule AB may be described schematically as

$$\mathrm{Rg}^* + AB \leftrightarrow [\mathrm{Rg}AB]^* \rightarrow [\mathrm{Rg}AB]^+ + e^-,$$

where the excited molecule $[\mathrm{Rg}AB]^*$ autoionizes instantly to form a nascent ionic complex. The emitted electron takes most of the available energy $E_0 = E^* - E^+$, while a portion of it is deposited in rovibrational levels of the nascent ion.

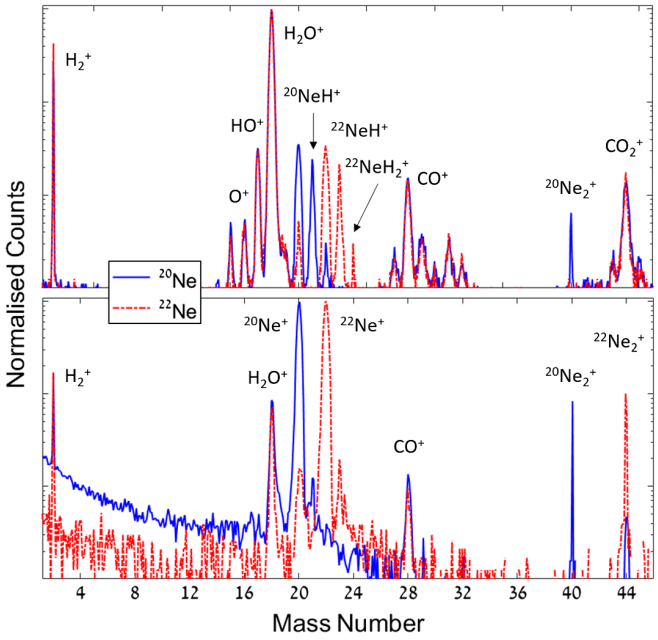

FIG. 3. Mass spectra of recoiling ions from collisions with trapped neon isotopes. Counts are presented in logarithmic scale and normalized to the highest peak. The top spectrum was taken at low trap density and is dominated by thermal intertrap collisions. The bottom spectrum was taken at high trap density and ultrahigh vacuum, and is dominated by ultracold, intratrap collisions.

The resulting ionic complex may remain intact, in which case the entire process is called AI, or dissociate to a number of possible channels [33],

$$\begin{aligned}[\mathrm{Rg}AB]^+ &\rightarrow \mathrm{Rg} + AB^+ \quad (\mathrm{PI}) \\ &\rightarrow \mathrm{Rg}A + B^+ \quad (\mathrm{RI}) \\ &\rightarrow \mathrm{Rg} + A + B^+ \quad (\mathrm{DI}).\end{aligned}$$

These are labeled PI, rearrangement ionization (RI), and dissociation ionization (DI). Considering both cold collisions within the trap (intratrap) and with thermal background gasses (intertrap), all of the aforementioned reactions are present in our system. Figure 3 presents the mass-calibrated time-of-flight spectrum of recoil ions detected when trapping $^{20}Ne^*$ or $^{22}Ne^*$.

At moderate vacuum conditions, and low trap density, water peaks are prominent, due to the large ionization cross section of H_2O-Ne^*, resulting from their strong attraction [34]. We checked that the BRs for ions resulting from Ne^*-H_2O collisions are stable with changing laser power, detuning, magnetic field strength, and by alternating between $^{20,22}Ne$. These are reported in Table I, and are in superb agreement with [35], who utilized a crossed-beam technique. In accordance with [35], no evidence (BR $< 0.1\%$) was found for AI, indicated by the lack of NeH_2O^+ ions.

TABLE I. Branching ratios for ionizing collisions between Ne^* and H_2O molecules. The neon isotope mass number and average collision energy are tabulated.

Mass number	E_{avg} meV	H_2O^+ %	HO^+ %	O^+ %	References
20	17	96.2(5)	3.3(5)	0.46(3)	This work
22	18	96.8(5)	2.8(5)	0.45(10)	This work
20 + 22	55	96.2(9.6)	3.2(5)	0.6(1)	[2,36]
20 + 22	70	96.7	2.9	0.4	[35]

The trap density is many orders of magnitude higher than the Ne^* background and so neon ions and dimers result solely from intratrap collisions. In the presence of a strong, near-resonant, light field, half of the atoms are in the $^3D_3$ excited state, where they experience a strong attraction to the metastable $^3P_2$ state, due to the resonant dipole-dipole interaction between them. In these optically assisted collisions, portrayed in Fig. 1, the two atoms are accelerated toward small internuclear distances where the probability of ionization is significantly larger. This process increases the collision rates by 2 orders of magnitude [11].

From mass spectra similar to Fig. 3, we find that the presence of near-resonant laser light increased the formation of dimers by at least a factor of 2, providing strong evidence for photoassociation in cold neon collisions (see Supplemental Material [37], which includes Refs. [38–40], for a discussion on the extraction of branching ratios). This enhancement is qualitatively understood from the process portrayed in Fig. 1, where the accelerated dimer at the potential $V^*(R)$ has a larger probability of reaching a small internuclear distance of roughly 4 a.u. where the ionic potentials $V^+(R)$ become strongly attractive, leading to positive difference potentials that promote association. The branching ratios for the creation of neon dimer ions are presented in Table II along with collision rates from the literature, and compared with results for trapped metastable helium. Previous investigations into optical collisions in neon traps, by [41] and [11], did not detect PI and AI separately.

The MOT-VMI enables high-resolution detection of the recoil energy distribution of penning ions from ultracold

TABLE II. Branching ratios and rates for ionizing collisions between trapped metastable atoms. K_{gg} is the two-body total ionization rate between ground state atoms. K_{ge} is taken at near-resonant light conditions, where reactive collisions occur predominantly between ground and excited state atoms.

	K_{gg} cm^3/s	K_{ge} cm^3/s	References
$Ne_2^+ + Ne^+$	$4(1) \times 10^{-10}$	$2.0(3) \times 10^{-8}$	[8,11]
Ne_2^+/Ne^+	<2.5%	5.1(1)%	This work
$He_2^+ + He^+$	$1.0(2) \times 10^{-10}$	$1.3(3) \times 10^{-8}$	[9,42]
He_2^+/He^+	3.0(3)%	16(2)%	[13]

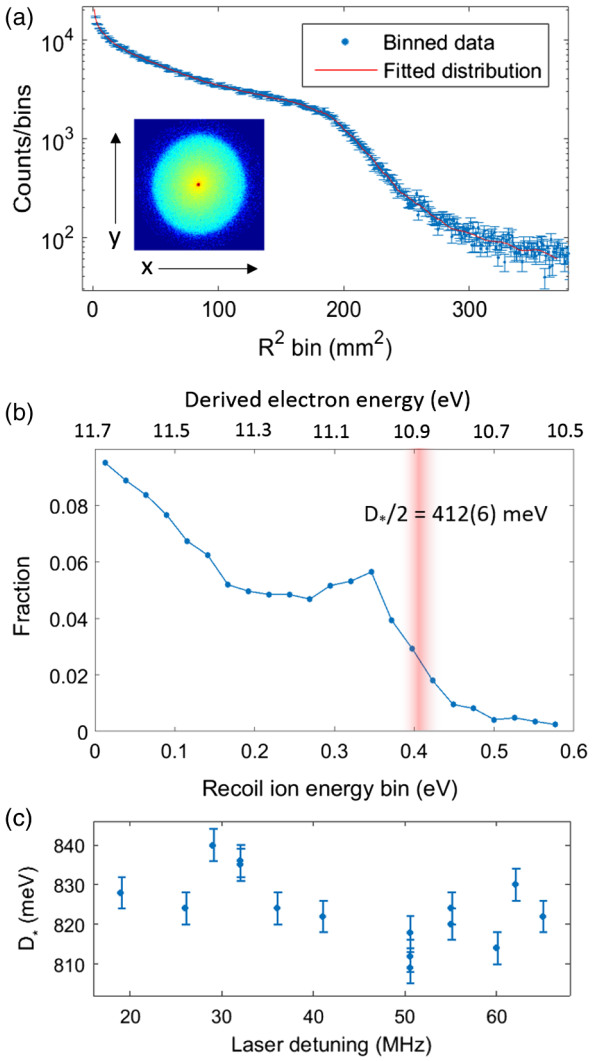

FIG. 4. (a) Distribution of squared hit radii from two-dimensional image on the detector plane (inset). The solid line indicates the best fit from the inversion process. (b) Energy spectrum of Ne^+ ions emerging from the $(Ne_2)^*$ collision complex, as extracted from fitting the radial hit distribution (see Supplemental Material, which includes Ref. [50], for further discussion on the inversion method). Electron energies derived from Eq. (1) are indicated, as well as the resulting well depth D_*. (c) Determined well depth for various red detuning of the trapping laser.

collisions. An example of this, taken without coincidence detection, with 100 times less water background, and ×200 denser trap, as compared to the conditions of Fig. 3 top, is shown in Fig. 4. Since the reactants are cold, the penning ion kinetic energy E_i is equal to half of the missing energy of the penning electrons [43],

$$E_i = (E_0 - E_e)/2. \tag{1}$$

Thus, it offers a high-resolution window, free of the $E_0 =$ 12 eV offset, into the quantum-governed dynamics of the penning ionization process. As shown in Fig. 1, the lowest energy electrons, which correspond to the highest energy ions, result from ionization near the minimum $E_0 - \epsilon$ of the difference potential $V^* - V^+$. Following the recipe of [44,45] usually applied to electron spectra, and utilizing Eq. (1), $\epsilon/2$ may be extracted in a straightforward manner from the 44% edge at the high energy side of the penning ion distribution [Fig. 4(b)]. To extract information on V^*, we utilize the consistency between various estimations of the location of minima of V^*, at $R_{\min} = 6.0$–6.5 a.u. [46,47], and the observation that the well-known ionic potentials do not vary substantially from 0 around $R_{\min}$ [48,49]. Thus the well depth of lowest potential may be evaluated directly from

$$D_* = \epsilon - V^+(R_{\min}) \approx \epsilon, \tag{2}$$

The results of various determinations of D_* are presented in Fig. 4(c), where they are found to not vary substantially with laser detuning. This observation further indicates that most optical ionization collisions in neon occur after the spontaneous emission of a photon, in contrast with the case for He^* [13], which has a longer lived excited state and a smaller mass (see Supplemental Material [37], which includes Refs. [51,52], for further discussion on the probability for spontaneous emission).

We estimate the uncertainty of the most repulsive $V^+(R_{\min})$ as 10 meV resulting from the uncertainty in $R_{\min}$ and conclude that the deepest potential depth for $Ne^*(^3P_2)$-$Ne^*(^3P_2)$ is $D_* = 824(22)$ meV. Kotochigova *et al.* [47] utilized a nonrelativistic multiconfiguration valence-bond method to calculate these potentials at short range *ab initio*. They report that the deepest attractive potential, labeled $^1\Delta_\sigma$, has a well depth of $D_* = 437$ meV, in strong disagreement with our findings. This discrepancy is to some extent resolved when considering approximate short-range potentials based on Na_2 developed by [46], where the inclusion of spin-orbit interactions increased the well depths by roughly 300 meV. Our result is compared with similar collisional systems in Table III.

TABLE III. Experimental well depths D_*, in meV, of the lowest diatomic potentials in Ne^*-Ne^* collisions, and similar systems.

	$He^*(2s^3S)$	$Ne^*(3s^3P_2)$	$Li(2s^2S)$	$Na(3s^2S)$
$He^*(2s^3S)$	850(90)[a]	500(100)[b]	868(20)[c]	740(25)[c]
$Ne^*(3s^3P_2)$	500(100)[b]	824(22)[d]	798(30)[e]	678(18)[f]
$Ar^*(4s^3P_2)$		300(50)[g]		602(23)[f]

[a]Estimation based on [43].
[b]Reference [53].
[c]Reference [54].
[d]This work.
[e]Reference [55].
[f]Reference [56].
[g]Reference [57].

To conclude, we successfully implemented a simple, versatile, MOT-VMI device, and demonstrated a few of its applications by conducting precise measurements of branching ratios and energy spectra of recoil ions emerging from inter- and intratrap collisions. The branching ratios for ionizing process in metastable neon colliding with water molecules are in superb agreement with those measured in crossed-beam experiments and may be beneficial for advancing the understanding of the penning ionization processes in planetary atmospheres [2]. Through the increase in the branching ratio for associative ionization in the presence of the trapping laser, we find long-sought evidence for photoassociation processes in noble gasses other than helium. Utilizing the imaging capabilities and a fast and simple inversion scheme, we obtain the energy distribution of recoil neon ions from cold optical collisions within the trap. The well depth of the lowest, highly excited molecular potential is extracted, and disagrees with non-relativistic *ab initio* calculations, demonstrating the dramatic effect of spin-orbit coupling, and the necessity of including relativistic effects in *ab initio* calculations of highly excited molecular potentials. The simplicity of construction, operation, and data analysis of the MOT-VMI makes it a compelling new tool for investigations of reactive processes in ultracold chemistry, and coherent control of the outcome of ionizing collisions [23,58,59].

Our entire system is located above the beamline of the Soreq Applied Research Accelerator [32], and we intend to utilize the MOT-VMI for precision measurements of recoil ions from the beta-decay of short-lived neon isotopes, in search of new physics in the weak sector of the standard model [60].

The work presented here is supported by grants from the Pazy Foundation (Israel), Israel Science Foundation (Grants No. 139/15 and No. 1446/16), and the European Research Council (Grant No. 714118 TRAPLAB). B. O. is supported by the Ministry of Science and Technology, under the Eshkol fellowship.

*ben.ohayon@mail.huji.ac.il

[1] D. Gerlich, P. Jusko, Š. Roučka, I. Zymak, R. Plašil, and J. Glosík, Astrophys. J. **749**, 22 (2012).
[2] S. Falcinelli, F. Pirani, and F. Vecchiocattivi, Atmosphere-Ocean **6**, 299 (2015).
[3] A. P. van der Poel and H. L. Bethlem, EPJ Tech. Instrum. **5**, 6 (2018).
[4] H. J. Metcalf and P. Van der Straten, *Laser Cooling and Trapping* (Springer-Verlag, New York, 1999).
[5] W. Vassen, C. Cohen-Tannoudji, M. Leduc, D. Boiron, C. I. Westbrook, A. Truscott, K. Baldwin, G. Birkl, P. Cancio, and M. Trippenbach, Rev. Mod. Phys. **84**, 175 (2012).
[6] D. Hauser, S. Lee, F. Carelli, S. Spieler, O. Lakhmanskaya, E. S. Endres, S. S. Kumar, F. Gianturco, and R. Wester, Nat. Phys. **11**, 467 (2015).
[7] W. Skomorowski, Y. Shagam, E. Narevicius, and C. P. Koch, J. Phys. Chem. A **120**, 3309 (2016).
[8] S. J. M. Kuppens, J. G. C. Tempelaars, V. P. Mogendorff, B. J. Claessens, H. C. W. Beijerinck, and E. J. D. Vredenbregt, Phys. Rev. A **65**, 023410 (2002).
[9] R. J. W. Stas, J. M. McNamara, W. Hogervorst, and W. Vassen, Phys. Rev. A **73**, 032713 (2006).
[10] H. C. Busch, M. K. Shaffer, E. M. Ahmed, and C. I. Sukenik, Phys. Rev. A **73**, 023406 (2006).
[11] R. Glover, J. Calvert, D. Laban, and R. Sang, J. Phys. B **44**, 245202 (2011).
[12] A. S. Flores, W. Vassen, and S. Knoop, Phys. Rev. A **94**, 050701(R) (2016).
[13] H. C. Mastwijk, J. W. Thomsen, P. van der Straten, and A. Niehaus, Phys. Rev. Lett. **80**, 5516 (1998).
[14] J. Deiglmayr, A. Grochola, M. Repp, K. Mörtlbauer, C. Glück, J. Lange, O. Dulieu, R. Wester, and M. Weidemüller, Phys. Rev. Lett. **101**, 133004 (2008).
[15] J. L. Carini, J. A. Pechkis, C. E. Rogers, P. L. Gould, S. Kallush, and R. Kosloff, Phys. Rev. A **87**, 011401(R) (2013).
[16] N. Bibelnik, S. Gersten, A. B. Henson, E. Lavert-Ofir, Y. Shagam, W. Skomorowski, C. P. Koch, and E. Narevicius, Mol. Phys. **117**, 2128 (2019).
[17] C. Cop and R. Walser, Phys. Rev. A **97**, 012704 (2018).
[18] D. G. Cocks, I. B. Whittingham, and G. Peach, Phys. Rev. A **99**, 062712 (2019).
[19] P. E. Siska, Rev. Mod. Phys. **65**, 337 (1993).
[20] R. Dörner, V. Mergel, O. Jagutzki, L. Spielberger, J. Ullrich, R. Moshammer, and H. Schmidt-Bcking, Phys. Rep. **330**, 95 (2000).
[21] A. T. J. B. Eppink and D. H. Parker, Rev. Sci. Instrum. **68**, 3477 (1997).
[22] D. W. Chandler, P. L. Houston, and D. H. Parker, J. Chem. Phys. **147**, 013601 (2017).
[23] C. A. Arango, M. Shapiro, and P. Brumer, Phys. Rev. Lett. **97**, 193202 (2006).
[24] J. Behr and G. Gwinner, J. Phys. G **36**, 033101 (2009).
[25] R. M. Yee *et al.*, Phys. Rev. Lett. **110**, 092501 (2013).
[26] R. Brédy, H. Nguyen, H. Camp, X. Fléchard, and B. DePaola, Nucl. Instrum. Methods Phys. Res., Sect. B **205**, 191 (2003).
[27] M. Weger, J. Maurer, A. Ludwig, L. Gallmann, and U. Keller, Opt. Express **21**, 21981 (2013).
[28] N. Kling, D. Paul, A. Gura, G. Laurent, S. De, H. Li, Z. Wang, B. Ahn, C. Kim, T. Kim *et al.*, J. Instrum. **9**, P05005 (2014).
[29] B. DePaola, R. Morgenstern, and N. Andersen, Adv. At. Mol. Opt. Phys. **55**, 139 (2008).
[30] J. Blieck, X. Fléchard, A. Cassimi, H. Gilles, S. Girard, and D. Hennecart, Rev. Sci. Instrum. **79**, 103102 (2008).
[31] B. Ohayon and G. Ron, Rev. Sci. Instrum. **86**, 103110 (2015).
[32] I. Mardor, O. Aviv, M. Avrigeanu, D. Berkovits, A. Dahan, T. Dickel, I. Eliyahu, M. Gai, I. Gavish-Segev, S. Halfon *et al.*, Eur. Phys. J. A **54**, 91 (2018).
[33] R. Sanders and E. Muschlitz, Int. J. Mass Spectrom. Ion Phys. **23**, 99 (1977).

[34] B. G. Brunetti, P. Candori, S. Falcinelli, F. Pirani, and F. Vecchiocattivi, J. Chem. Phys. **139**, 164305 (2013).
[35] N. Balucani, A. Bartocci, B. Brunetti, P. Candori, S. Falcinelli, F. Palazzetti, F. Pirani, and F. Vecchiocattivi, Chem. Phys. Lett. **546**, 34 (2012).
[36] S. Falcinelli, M. Rosi, F. Pirani, D. Stranges, and F. Vecchiocattivi, J. Phys. Chem. A **120**, 5169 (2016).
[37] See Supplemental Material at http://link.aps.org/supplemental/10.1103/PhysRevLett.123.063401 for a discussion on the probability of spontaneous emissions, the extraction of branching ratios for various laser intensities, and details regarding the inversion process.
[38] J. Oberheide, P. Wilhelms, and M. Zimmer, Meas. Sci. Technol. **8**, 351 (1997).
[39] B. Ohayon, H. Rahangdale, A. J. Geddes, J. C. Berengut, and G. Ron, Phys. Rev. A **99**, 042503 (2019).
[40] B. Ohayon, E. Wåhlin, and G. Ron, J. Instrum. **10**, P03009 (2015).
[41] W. J. Van Drunen, Ph.D. thesis, Technische Universität Darmstadt (2008).
[42] P. J. J. Tol, N. Herschbach, E. A. Hessels, W. Hogervorst, and W. Vassen, Phys. Rev. A **60**, R761 (1999).
[43] M. Pieksma, M. Cizek, J. W. Thomsen, P. van der Straten, and A. Niehaus, Phys. Rev. A **66**, 022703 (2002).
[44] W. H. Miller, J. Chem. Phys. **52**, 3563 (1970).
[45] H. Hotop, Radiat. Res. **59**, 379 (1974).
[46] M. R. Doery, E. J. D. Vredenbregt, S. S. Op de Beek, H. C. W. Beijerinck, and B. J. Verhaar, Phys. Rev. A **58**, 3673 (1998).
[47] S. Kotochigova, E. Tiesinga, and I. Tupitsyn, Phys. Rev. A **61**, 042712 (2000).
[48] D. Trevor, J. Pollard, W. Brewer, S. Southworth, C. Truesdale, D. Shirley, and Y. Lee, J. Chem. Phys. **80**, 6083 (1984).
[49] A. Carrington, D. I. Gammie, J. C. Page, A. M. Shaw, and J. M. Hutson, J. Chem. Phys. **116**, 3662 (2002).
[50] B. J. Whitaker, *Imaging in Molecular Dynamics: Technology and Applications* (Cambridge University Press, Cambridge, England, 2003).
[51] M. R. Doery, E. J. D. Vrendenbregt, J. G. C. Tempelaars, H. C. W. Beijerinck, and B. J. Verhaar, Phys. Rev. A **57**, 3603 (1998).
[52] A. Gallagher and D. E. Pritchard, Phys. Rev. Lett. **63**, 957 (1989).
[53] R. Neynaber and S. Tang, J. Chem. Phys. **72**, 5783 (1980).
[54] H. Hotop, T. Roth, M.-W. Ruf, and A. Yencha, Theor. Chem. Acc. **100**, 36 (1998).
[55] J. Lorenzen, H. Hotop, and M. W. Ruf, Z. Phys. D **1**, 261 (1986).
[56] S. Schohl, M. W. Müller, H. A. J. Meijer, M.-W. Ruf, H. Hotop, and H. Morgner, Z. Phys. D **16**, 237 (1990).
[57] R. Neynaber and S. Tang, J. Chem. Phys. **72**, 6176 (1980).
[58] J. L. Carini, S. Kallush, R. Kosloff, and P. L. Gould, Phys. Rev. Lett. **115**, 173003 (2015).
[59] J. J. Omiste, J. Floß, and P. Brumer, Phys. Rev. Lett. **121**, 163405 (2018).
[60] B. Ohayon, J. Chocron, T. Hirsh, A. Glick-Magid, Y. Mishnayot, I. Mukul, H. Rahangdale, S. Vaintraub, O. Heber, D. Gazit *et al.*, Hyperfine Interact. **239**, 57 (2018).